UNIVERSIDAD DE CANTABRIA

Departamento de Ingeniería de Comunicaciones

TESIS DOCTORAL

Cryogenic Technology in the Microwave Engineering: Application to MIC and MMIC Very Low Noise Amplifier Design

Juan Luis Cano de Diego

Santander, Mayo 2010

Chapter II
Cryogenic Technology Applied to Microwave Engineering

Cryogenics can be defined as the study of production of extremely low temperatures, below -150 ºC (123.15 kelvin), and the materials behavior under such conditions. These low temperatures make more convenient the use of the absolute scale of temperatures, which unit is kelvin (K), instead of the more common Celsius (ºC) or Fahrenheit (ºF) scales [2.1], [2.2]. Conversion between scales is straightforward following (2.1) and (2.2).

$$T(K) = T(^{o}C) + 273.15 \qquad (2.1)$$

$$T(K) = [T(^{o}F) + 459.67]/1.8 \qquad (2.2)$$

In the microwave engineering field, the main application of cryogenics is related with the reduction of thermal noise in cooled high sensitivity receivers used in radioastronomy and space missions. The need of cooling down these systems, or a part of them, is what takes microwave engineers to go into cryogenics field of knowledge; which requires a great researching effort to gain knowledge in areas far from their professional training.

This chapter gives an introduction to these concepts, relating them to a practical view and their application to the assembly and set up of the cryogenic systems available in the DICOM. The theory of the typical cryogenic system work is explained and some practical aspects are presented, which make the system operative for usual microwave applications.

2.1. Description of the Gifford-McMahon Cooling System

In the DICOM there are currently two independent cryogenic systems based on the Gifford-McMahon cooling cycle [2.2]-[2.4]. The coolant, which is Helium in its gas phase (boiling point, T_b = 4.22 K), follows a cyclical path in the refrigerator, which steps can be explained using the basic cylinder-and-piston sketch of Fig. 2.1a.
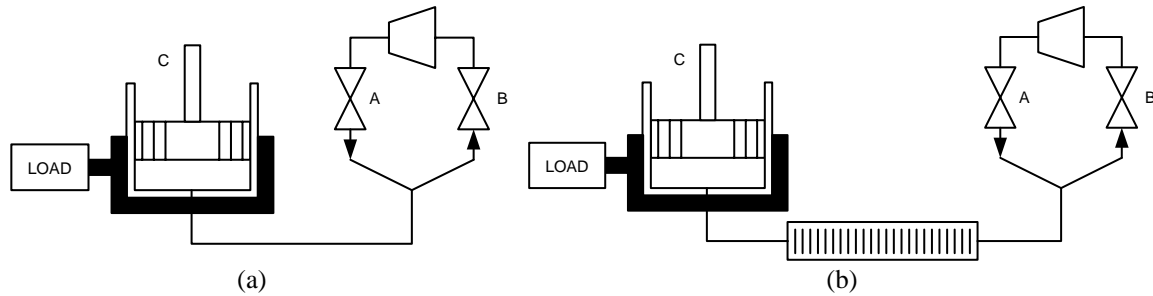

Fig. 2.1. Sketch of the cooling system indicating inlet valve (A), exhaust valve (B) and piston inside the cylinder (C): (a) without regenerator matrix; (b) with regenerator matrix.

A compressed gas source is connected to the bottom of cylinder *C* through an inlet valve *A*. Valve *B* is in the exhaust way to the low pressure area in the compressor. With the piston at the bottom of cylinder, and with the valve *B* closed and valve *A* open, the piston moves upward and the cylinder fills up with compressed gas. When inlet valve is closed and exhaust valve open, the gas expands in the exhaust pipe and then cools the load. The resulting temperature gradient along the cylinder walls produces a heat flow from the load to the cylinder. As a result of this, the gas heats up to its original temperature. Now, with the exhaust valve open and inlet valve closed, the piston descends, displacing the remaining gas to the exhaust pipe, and the cycle restarts.

This basic system cannot produce the extreme low temperatures needed in a cryogenic system. Therefore, the incoming gas must be cooled with the exhaust gas before entering the cylinder. This is made through a regenerator matrix, see Fig. 2.1b, which removes heat from the incoming gas, stores it and then releases it to the exhaust gas.

The regenerator is an inverse heat flow exchanger through which the Helium goes alternatively in each direction. It is covered with a material with a large surface, high specific heat, and low thermal conductivity, which easily accepts heat (if the Helium temperature is higher) and transmits to Helium (if its temperature is lower). In a stationary state, a system like this follows the temperature profile of Fig. 2.2 [2.5].
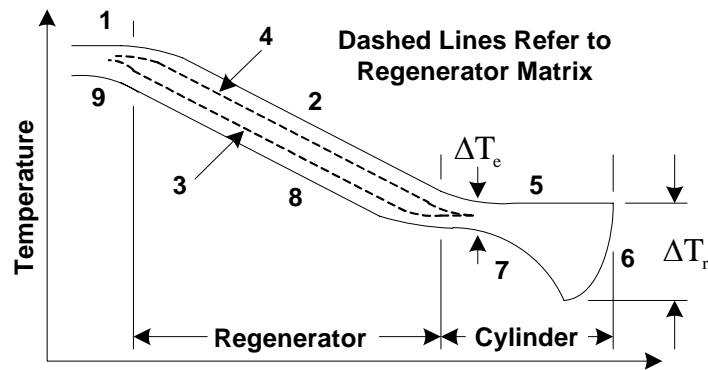
Fig. 2.2. Temperature profile of a one-stage refrigerator.

With the piston at the bottom end, the compressed gas goes through the inlet valve *A* at room temperature, RT, $T \sim 296$ K (number 1 in Fig. 2.2). While the piston goes up, the gas goes through the regenerator so the matrix absorbs heat (it heats up from number 3 to number 4), and the gas cools down (number 2). At the original pressure, the cooled gas fills the volume under the piston. At this point, the gas temperature is approximately equal to the load temperature (number 5). Then, inlet valve is closed and exhaust valve open, enabling the gas to expand and cool down even more (number 6). The temperature drop, ΔT_r, is the responsible of the cooling effect. Now, the heat flows from the load to the cylinder walls, heating up the gas to a temperature slightly lower than it had when it entered in the cylinder (number 7). As the gas passes through the regenerator it heats up again, since it receives heat from the matrix (number 8), and the matrix cools down again (from number 4 to number 3). Finally, the low pressure gas leaves the system through exhaust valve *B* at RT approximately (number 9).

In the system of Fig. 2.1b, the piston must be hermetically sealed to avoid pressure loss and should be designed to bear non balanced forces as well. A more practical version of this cycle is shown in Fig. 2.3a. This system includes a cylinder with two ends and an elongated piston made of a low thermal conductivity material.
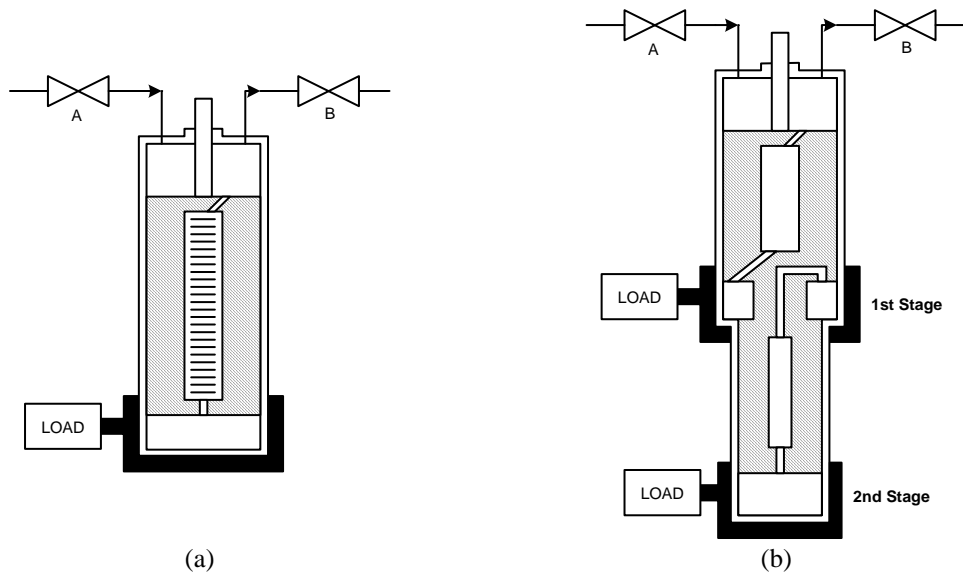
Fig. 2.3. Improved versions of the refrigerator: (a) one-stage; (b) two-stage.

Since the pressure at both ends of the cylinder is approximately equal, there is no need to have a sealed piston. Now the piston just displaces gas from one cylinder end to the other, therefore no mechanical work is made. The piston becomes a displacer. The regenerator is placed inside the piston to reduce hardware and also to minimize heat losses.

The refrigerator shown in Fig. 2.3a can achieve temperatures in the range 30-77 K. Since the applications where these systems are used need lower temperatures is needed to add more stages. The addition of a second stage enables to reach temperatures down to 6 K, Fig. 2.3b. The systems available in the DICOM laboratories are of this second type.

2.2. Description of the Cryogenic Systems at DICOM Laboratories

The lowest temperatures in the systems described in the previous section only can be reached under ideal conditions. That is, the thermal load that affects the system, through any of the heat transmission ways, is minimal and also the pressure conditions are optimal, with a high quality vacuum.

In real applications, everything that is added to the system to be measured produces an increase of the thermal load, moreover, if special care is not taken during the cryostat hardware design process, this thermal load will be increased as well, even if the device under test (DUT) is the same.

The person in charge of purchasing the cryogenic system has to face up many different problems. First of all is to size up the system requirements. Since the thermal load, with units of watts, and the minimum reachable temperature are related, there is

only need to calculate the first one and then to purchase a system that fulfills the second one. An ideal solution would be to buy the most powerful available system but in most situations this would produce a budget problem.

As a rule, cryogenic system manufacturers give some plots that relate both variables both in the first and second stages, which facilitate the system model choice. In Fig. 2.4 two examples of these plots for commercially available systems are presented.
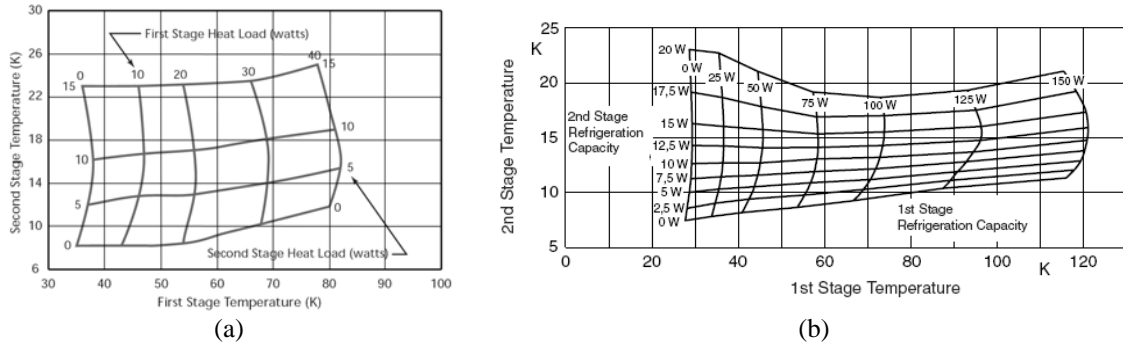

(a)   (b)

Fig. 2.4. Refrigeration power at 60 Hz of the systems: (a) model 1020 from CTI Cryogenics [2.6]; (b) model Coolpower 10MD from Leybold [2.7].

The available systems at DICOM have been purchased from *Advanced Research Systems (ARS),* which does not provide such plots. On the other hand, they give some data presented in Table 2.1 [2.8].

	Model	
	DE-202AF	DE-210AE
Minimum Temp. (K)	< 9	< 9
Cooling Power (2nd stage)	0.5W @ 10K	4W @ 10K
	2.5W @ 20K	17W @ 20K
Cooling Power (1st stage)	4W @ 77K	60W @ 77K
Cooling Time down to 20 K	45 min.	40 min.
Cooling Time down to minimum temperature	80 min.	80 min.

Table 2.1. Specifications of the available cryogenic systems working at 60 Hz.

Each system is joined to its cryostat box, usually called Dewar[1], where the different measurement tests are performed. Dewars are made up of many pieces designed to keep the vacuum, with the lowest leakage rate possible and, at the same time, to present different temperature stages, in order to minimize the temperature gradient between consecutive stages. Otherwise the thermal load would be huge

---

[1] The box where the tests are performed in a cryogenic system usually is known as Dewar, in honor to James Dewar, an English scientist who developed at the end of XIX century the first versions of a vacuum vessel made of glass and thermally isolated [2.4].

preventing the system to work properly. It is important to note that the models purchased from ARS refer to the cold-head, compressor and vacuum pump. All the hardware needed for completing the system has to be designed and manufactured by the end user.

The exploded view of the cryogenic system, made up of the cryostat cold-head and the Dewar, is presented for the model DE-210AE in Fig. 2.5, being very similar for the other system. Elements 6, 8, 17 and 18 build the Dewar; elements 3, 9, 13 and 14 form the radiation shield in the first stage; and element 11 is the second stage base where the circuits are attached. All the components in Fig. 2.5, except the cold head, have been designed during this work at the DICOM following guidelines from previous designs [2.9] based on a design from NRAO[2]. Drawings of the different parts comprising the cryogenic system can be found in Annex I.

The effect of these parts in the thermal load is shown in next section where the calculations to obtain the total thermal load for the system planning are detailed.

2.3. Thermal Load Calculation

To obtain the total thermal load in the system four different mechanisms have to be considered: heat conduction through the coaxial and DC-bias cables, heat radiation between surfaces at different temperatures, heat conduction by the residual gas inside the Dewar, and dissipation due to circuits power consumption.

2.3.1. Conduction thermal load calculation

Cryogenic systems involve great temperature gradients. Since the thermal conductivity of materials is variable with temperature, the integral of the thermal conductivity over the temperature range has to be calculated [2.2], [2.3]. The general equation for calculating the heat transfer by one-dimension conduction, between temperatures T_1 and T_2, is given by (2.3).

$$Q = \frac{-1}{\int_{x_1}^{x_2} \frac{dx}{A(x)}} \left[\int_{T_1}^{T_2} K(T)dT \right] \qquad (2.3)$$

---

[2] National Radio Astronomy Observatory, 22903-2475, Charlottesville, VA, USA.
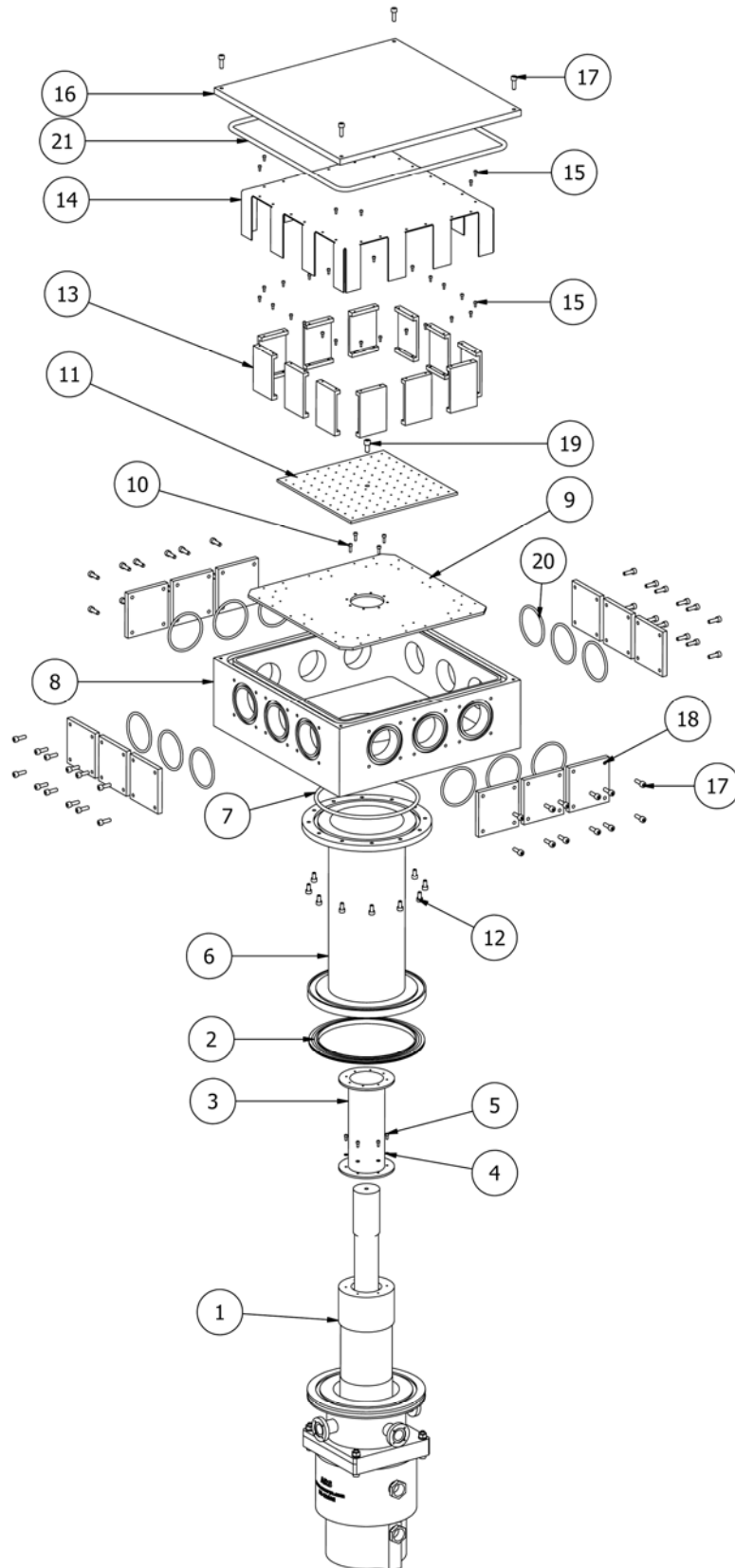
Fig. 2.5. Exploded view of the cryogenic system: 1. cold-head model DE-210AE; 2. centering ring; 3. first stage support; 4. washers; 5. screws; 6. Dewar support; 7. o-ring; 8. Dewar; 9. radiation shield base; 10. screws; 11. second stage base; 12. screws; 13. radiation shield supports; 14. radiation shield; 15. screws; 16. dewar cover; 17. screws; 18. Dewar window cover; 19. screw; 20. o-ring; 21. o-ring.

Where $K(T)$ is the material thermal conductivity (W/mK), $A(x)$ is the conductor cross section (m^2), T_2 is the higher temperature (K), and T_1 the lower temperature (K). The minus sign is a convention since the heat flow is defined as opposite to temperature gradient; for this reason it will be omitted in the following calculations. Equation (2.3) can be rearranged as (2.4)

$$Q = \frac{A}{L}\left[\int_0^{T_2} K(T)dT - \int_0^{T_1} K(T)dT\right] \qquad (2.4)$$

Where L is the conductor length (m). This equation has to be applied in each element going into the Dewar, generally coaxial and DC-bias cables. According to (2.3), small-section and long cables made of low thermal conductivity materials are preferable. For coaxial cables, stainless-steel outer and inner conductor is the best option. If losses are a concern, BeCu (Beryllium-Copper) inner conductor may be selected.
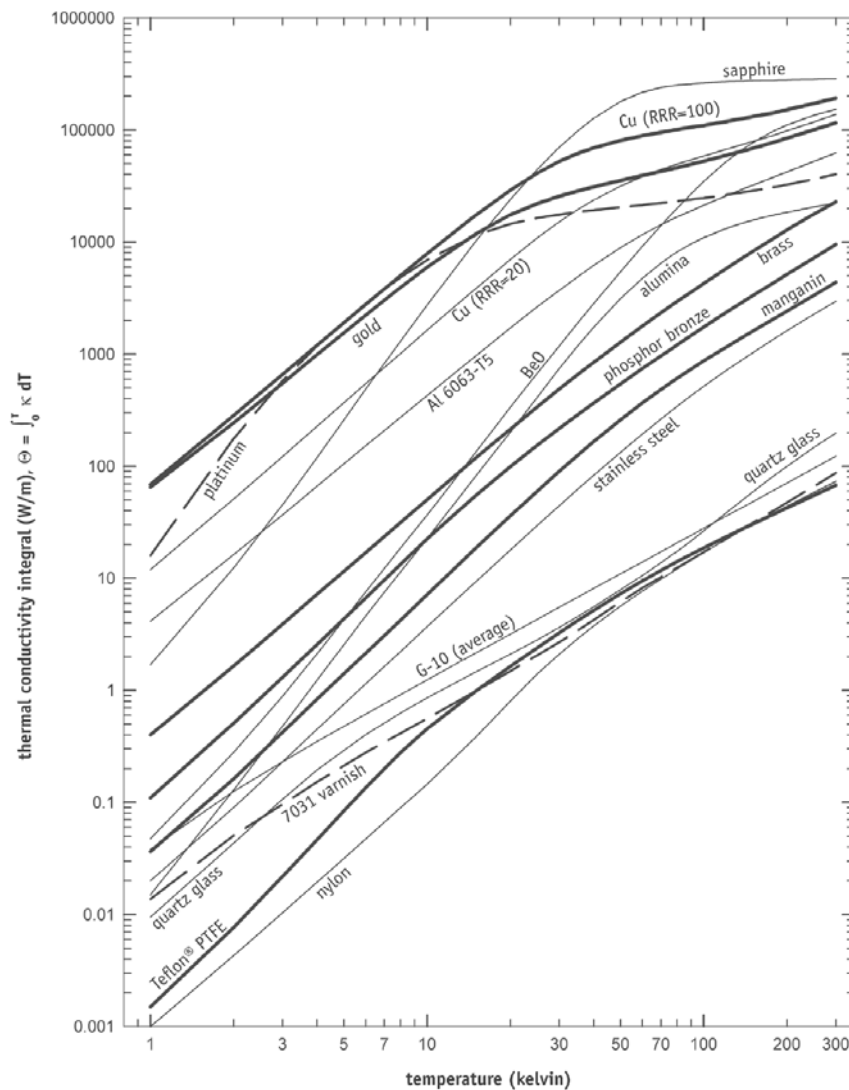

Fig. 2.6. Thermal conductivity integral of common materials in cryogenics [2.10].

Plots of the thermal conductivity integrals for common materials are published in the literature [2.2]-[2.4]. Moreover, the National Institute of Standards and Technology, *NIST*, provides equations for the thermal conductivity of common materials [2.11]. These equations are fitted polynomials or logarithmic polynomials with many coefficients to cover a wide range of temperatures.

General form of the thermal conductivity equation is given by (2.5).

$$\log(K(T)) = a + b\log T + c(\log T)^2 + d(\log T)^3 + e(\log T)^4 + ... \\ ... + f(\log T)^5 + g(\log T)^6 + h(\log T)^7 + i(\log T)^8$$

(2.5)

The coefficients of previous equation for the usual materials are presented in Table 2.2 and Table 2.3. The given (2.5) is not valid for the OFHC copper (Oxygen Free High Conductivity) so (2.6) applies.

$$\log(K(T)) = \frac{2.2154 - 0.88068T^{0.5} + 0.29505T - 0.048310T^{1.5} + 0.003207T^2}{1 - 0.47461T^{0.5} + 0.13871T - 0.020430T^{1.5} + 0.001281T^2}$$

(2.6)

Coefficient	Aluminum 6061 – T6	Aluminum 1100	Brass	Stainless Steel 304	Inconel 718	BeCu	Ti-6Al-4V
a	0.07918	23.39172	0.02103	-1.4087	-8.28921	-0.50015	-5107.8774
b	1.09570	-148.57330	-1.01835	1.3982	39.4470	1.93190	19240.422
c	-0.07277	422.19170	4.54083	0.2543	-83.4353	-1.69540	-30789.064
d	0.08084	-653.66640	-5.03374	-0.6260	98.1690	0.71218	27134.756
e	0.02803	607.04020	3.20536	0.2334	-67.2088	1.27880	-14226.379
f	-0.09464	-346.15200	-1.12933	0.4256	26.7082	-1.61450	4438.2154
g	0.04179	118.42760	0.17406	-0.4658	-5.72050	0.68722	-763.07767
h	-0.00571	-22.27810	-0.00382	0.1650	0.51115	-0.10501	55.796592
i	0	1.77019	0	-0.0199	0	0	0
Range	4-300 K	4-300 K	5-110 K	4-300 K	4-300 K	1-120 K	20-300 K

Table 2.2. Coefficients of thermal conductivity equation for metals.

Coefficient	Teflon®	Polyamide (Nylon®)	Polyamide (Kapton®)	G10 CR (norm)	G10 CR (warp)
a	2.7380	-2.6135	5.73101	-4.1236	-2.64827
b	-30.677	2.3239	-35.5199	13.788	8.80228
c	89.430	-4.7586	79.9313	-26.068	-24.8998
d	-136.99	7.1602	-83.8572	26.272	41.1625
e	124.69	-4.9155	50.9157	-14.663	-39.8754
f	-69.556	1.6324	-17.9835	4.4954	23.1778
g	23.320	-0.2507	3.42413	-0.6905	-7.95635
h	-4.3135	0.0131	-0.27133	0.0397	1.48806
i	0.33829	0	0	0	-0.11701
Range	4-300 K	4-300 K	4-300 K	10-300 K	12-300 K

Table 2.3. Coefficients of the thermal conductivity equation for non metals.

Thermal load due to conduction comes, at the most, through the cables that go into the system, providing a direct way from the outside to the test area for the heat flow. Because to this, these cables should be thermally sunk, that is, to anchor them, by

means of a connection with high thermal conductivity, to the different intermediate stages in order to isolate the test area from the outside.

Apart from the material, the heat sink should be designed so the cable temperature gradient is negligible regarding the temperature of the cold stage which is attached to. In [2.2] a method for calculating the heat sink length, L_2 (see Fig. 2.7), as a function of environment temperatures and cable material, is presented. In this work only the results of this method, applied to the structure in Fig. 2.7, are shown in Table 2.4.
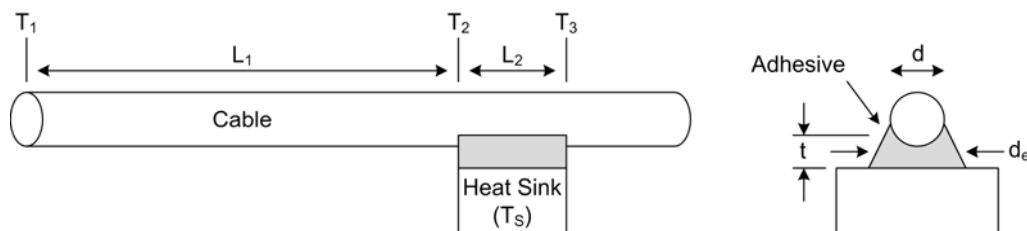

Fig. 2.7. Theoretic configuration of a heat sink.

| | T_1 | T_S | L_2 (mm) of heat sink for different wire sizes | | | |
| | | | 0.21 mm^2 | 0.032 mm^2 | 0.013 mm^2 | 0.005 mm^2 |
Material	(K)	(K)	(24 AWG)	(32 AWG)	(36 AWG)	(40 AWG)
Copper	300	80	160	57	33	19
	300	4	688	233	138	80
Phosphorus-	300	80	32	11	6	4
Bronze	300	4	38	13	7	4
Manganin	300	80	21	4	4	2
$Cu_{86}Mn_{12}Ni_2$	300	4	20	7	4	2
Stainless	300	80	17	6	3	2
Steel 304	300	4	14	5	3	2

Table 2.4. Heat sink length for cable anchoring down to temperature T with a temperature difference less than 1 mK.

Although the heat sinks presented in Fig. 2.7 may be useful for flexible cables such the ones used for DC biasing, the rigidity of these sinks is a problem when semi-rigid or rigid cables are needed, for example, in high frequency measurements. For this purpose, it is better to install heat sinks with a flexible and high thermal conductivity element joining the cable and the thermal anchor.
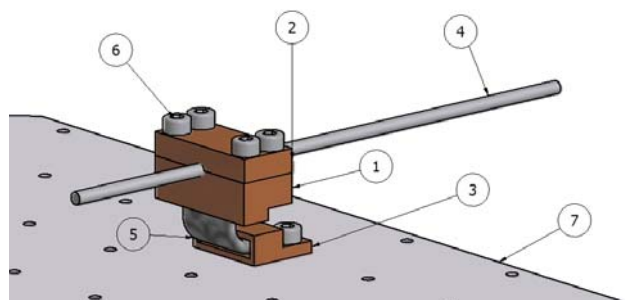

Fig. 2.8. Proposed heat sink for semi-rigid hardware; 1. Heat sink part A, 2. Heat sink part B, 3. Heat sink part C, 4. Semi-rigid coaxial cable, 5. Flexible tinned copper braid, 6. Screws, 7. Cooling base (first or second cryostat stage).

The heat sinks used in the cryogenic systems at DICOM follow the structure proposed in Fig. 2.8. The flexible element is made of tinned copper braid whereas the heat sink parts (A, B and C) are made of OFHC copper, which shows one of the best thermal conductivities. A small piece of Indium foil is advisable to be used at the heat sink – cable interface to improve surfaces contact.

In the following, the thermal load calculation, due conduction of coaxial and bias cables, is presented for the system DE-202AF, which has been used in the laboratory since the beginning of this work. It is important to note that, due to design errors overcome in the newer system, cables cannot be heat sunk to the cryostat first stage in the DE-202AF system; therefore, all the heat load falls on the second stage.

Coaxial cables used in this system are model PN052140 from ARS for measurements up to 50 GHz. These cables have the particularity that they use a sliding mechanism that enables to introduce a variable length of cable in the Dewar without affecting the vacuum inside. Total length of these cables is 46 cm, having, usually, around 20 cm inside the Dewar. For calculation purposes a cable length of 20 cm will be considered, with a temperature of 296 K at one end and 20 K at the other. The cable outer diameter is 2.2 mm, estimating an outer conductor thickness of 0.3 mm and an inner conductor diameter of 0.5 mm. To consider a worst case scenario, the inner conductor is supposed to be made of copper, which has a high thermal conductivity and therefore the thermal load will be higher. The outer conductor is known to be stainless steel. Outer conductor section is given by (2.7).

$$A_1 = \pi(2 \cdot r \cdot t + t^2) \tag{2.7}$$

Where $(r+t)$ is the outer conductor radii and $t = 0.3$ mm. Therefore, $A_1 = 1.8$ mm^2. Inner conductor section is $A_2 = 0.78$ mm^2. Applying (2.4) and taking into account the integrals of thermal conductivity for the referred materials given in Table 2.5, the thermal load for one cable is calculated, obtaining a value of 0.5 W.

	$\int_0^{300K} K(T)$	$\int_0^{20K} K(T)$
Stainless Steel	3000	18
Copper (RRR=20)	130000	6500

Table 2.5. Thermal conductivity integrals for coaxial cable materials.

Since two cables are needed, at least, for a measurement, the total thermal load generated by the coaxial cables due to conduction is 1 W.

About the DC-bias cables, they are made of copper with a diameter of 0.7 mm and length 48 cm. Cables section is $A = 0.5\ mm^2$, and therefore the thermal load produced for each cable is 0.13 W. Considering the use of five cables for DC biasing, then the thermal load is raised to 0.65 W.

Temperature sensors also need DC cables for biasing and signal reading. These cables go into the system through a connector in the lower end of the cryostat and then go up surrounding the cold head up to the test area. Therefore, they can be considered as thermally anchored to the coldest stage from the beginning and along their length. Thus, their thermal load is considered as negligible.

Including all the calculated effects, a total thermal load due to conduction of 1.65 W is estimated over the second stage.

2.3.2. Radiation thermal load calculation

When two bodies, at direct sight, are separated by an environment which does not absorb radiation an energy exchange occurs as a result of reciprocal emission and absorption processes. The net heat transfer rate from one surface at temperature T_1 to other at temperature T_2 can be calculated using (2.8) [2.3].

$$Q = \sigma \cdot A_1 \cdot F_A \cdot F_E (T_1^4 - T_2^4)$$ (2.8)

Parameter σ is the Stefan-Boltzmann's constant with value $5.67 \cdot 10^{-8}\ Wm^{-2}K^{-4}$. A_1 is the area of the inner surface; F_A is a shape and orientation factor relative to A_1 for both bodies; and F_E is the emission and absorption factor for both surfaces. If the surface of one body is small or is enclosed for the other surface (as it happens in the described cryogenic systems), then $F_A = 1$, otherwise this parameter must be evaluated. Parameter F_E is given by (2.9).

$$F_E = \frac{\varepsilon_1 \cdot \varepsilon_2}{\varepsilon_2 + \dfrac{A_1}{A_2}(1 - \varepsilon_2) \cdot \varepsilon_1}$$ (2.9)

Where ε_1 and ε_2 are the emissivities of the inner and outer surfaces respectively. These emissivities depend on the temperature and, to a great extent, on the surface finishing. Some orientative values of material emissivities are presented in Table 2.6 [2.12], since they have not been obtained at cryogenic temperatures.

Material	Emissivity (ε)
Aluminum	0.01-0.06
Aluminum very polished	0.02-0.08
Aluminum oxidized	0.11-0.22
Aluminum very oxidized	0.20-0.31

Copper	0.22
Copper very polished	0.02
Copper oxidized	0.78
Gold polished	0.02-0.03
Nickel polished	0.072
Nickel oxidized	0.59-0.86
Stainless Steel polished	0.075
Stainless Steel oxidized	0.85
Brass polished	0.03
Brass oxidized	0.6
Glass	0.9

Table 2.6. Emissivity of some common materials.

In general, aluminum and stainless-steel are chosen for Dewar manufacturing. Anyway, polished surfaces are preferable since the thermal load reduction, which has to be calculated both at first and second stage, is noticeable.

Finally, the area of the surfaces involved in the calculation has to be determined in order to obtain the total thermal load due to radiation. For calculating the load over the first stage, the inner wall of the Dewar (element number 8 in Fig. 2.5) is surface A_2, whereas the outer faces of the radiation shield (elements 9, 13 and 14 in Fig. 2.5) form surface A_1. In order to calculate the load over the second stage, the inner faces of the radiation shield make the surface A_2 and the cooling base (element 11 in Fig. 2.5) is the surface A_1.

For the system under consideration, inner walls of the Dewar have a total surface of 0.286 m^2, outer faces of the radiation shield have a total surface of 0.254 m^2, and the cooling base has a surface of 0.119 m^2. It is considered that the inner faces of the radiation shield have approximately the same surface as the outer faces.

All the hardware involved in these calculations is made of aluminum. Since it has not any special finishing, an emissivity of $\varepsilon = 0.1$ is used. Dewar is at RT whereas second stage is at 20 K. The radiation shield is considered to be at 80 K.

Using the data above, total thermal load due to radiation is 6.11 W over the first stage and 0.02 W over the second stage.

2.3.3. Conduction by residual gas thermal load calculation

Once the temperature inside the cryostat is low enough to produce the condensation of the remaining gas, the cryogenic vacuum is reached. In such situation, the heat exchanged by this kind of conduction is negligible. Therefore, in a well-designed system, in which pressures of 10^{-6} mbar can be easily reached, there is no need to calculate the thermal load due to conduction by residual gas. On the other hand, if leaks are present in the system, thermal load due to this process may be dominant over the other loads, making impossible to reach the desired low temperature. Equation

(2.10) [2.13] gives a simplified way to calculate the heat exchanged between two parallel surfaces of area A at temperatures T_1 and T_2 due to this effect.

$$Q = K_1 A \cdot a_0 \cdot P \cdot (T_1 - T_2)$$ (2.10)

Where P is the pressure of the remaining gas (Pascal), a_0 is a non-dimensional coefficient, and K_1 is a gas dependent constant. For air K_1 can be set to 1.2. The coefficient a_0 is always less than 1, so it can be set to 1 to consider a worst case scenario. Table 2.7 shows this calculation for different residual gas pressures at both stages.

Stage	Area (m^2)	Temp. (K)	P (mbar)	K_1	a_0	Q (W)
1ª stage	0.254	80	10^{-2}	1.2	1	65.8
2ª stage	0.119	20	10^{-2}	1.2	1	8.5
1ª stage	0.254	80	10^{-3}	1.2	1	6.58
2ª stage	0.119	20	10^{-3}	1.2	1	0.85
1ª stage	0.254	80	10^{-4}	1.2	1	0.658
2ª stage	0.119	20	10^{-4}	1.2	1	0.085
1ª stage	0.254	80	10^{-5}	1.2	1	0.0658
2ª stage	0.119	20	10^{-5}	1.2	1	0.0085

Table 2.7. Thermal load due to conduction by residual gas at different stages.

Applying (2.10) for different pressures at the system stages it can be stated that for pressures lower than 10^{-4} – 10^{-5} mbar this thermal load is negligible. This is an important result to take into account when selecting the vacuum pump for the system.

2.3.4. Dissipation thermal load calculation

Devices or circuits cooled in the cryostat are a source of heat since part of the energy they receive from bias lines is dissipated in the second stage, where the device under test is anchored. To obtain the thermal load in this case, DC power dissipated by the circuit must be calculated.

The experiment with highest DC bias consumption up to now in the laboratory was the measurement of a receiver system which was made up of two monolithic (MMIC) amplifiers with the following bias points: V_{dd1} = 3 V, I_{dd1} = 60 mA y V_{dd2} = 4 V, I_{dd2} = 60 mA. Therefore, the thermal load due to dissipation in this case is 0.42 W, which falls entirely over the second stage.

2.3.5. Summary of thermal load calculations

Table 2.8 shows the calculated thermal loads at both stages for the designed system of Fig. 2.5 considering a residual gas pressure of 10^{-5} mbar.

P = 10^{-5} mbar	1st Stage	2nd Stage
Conduction	0	1.65
Radiation	6.11	0.02
Residual Gas	0.065	0.008

Dissipation	0	0.42
Total	6.17 W	2.1 W

Table 2.8. Total thermal load of the designed cryogenic system at both stages.

According to calculations in Table 2.8 it is clear that only one of the systems considered in Table 2.1 fulfils the power requirements to achieve the desired temperatures. Thermal load in the first stage of model DE-202AF would be so high that this stage could not reach the temperature of 77 K, which would produce an increase in thermal load over second stage, preventing this stage to be cooled below 20 K. These results demonstrate the inability of the first system to work as expected and also the need of performing these calculations before acquiring a new system. To overcome these problems, a more powerful system, DE-210AE, was acquired by DICOM which enables fast cooling, reaching lower temperatures.

2.4. Additional Considerations about Designing Cryogenic Systems

2.4.1. Suitable materials for hardware manufacturing [2.14]

In previous calculations some characteristics of materials such thermal conductivity or emissivity have been taken into consideration, so the selection of materials is a concern when designing the system. For the Dewar, stainless-steel is commonly used since it shows some advantages over other materials. It does not suffer from oxidation and it is easily electro-polished, which reduces the effective surface and therefore the gas absorbed by the surface is reduced too. Another advantage is that it is easily solderable obtaining reliable high vacuum joints, which facilitates to produce home-made designs.

The main drawback of stainless-steel is its weight. When weight may be a problem, aluminum is the best option. Aluminum is more fragile so it needs more thickness to get the same rigidity as stainless-steel; even so the weight reduction is noticeable. The drawback of aluminum is that it is more prone to leaks in the joints, that is the reason why polishing and nickel-plating are advisable. Emissivity of nickel is constant whereas for aluminum it depends on the surface oxidation.

The radiation shield is needed in order to reduce the thermal load due to radiation from the outer stage at 296 K (Dewar) to the second stage at 20 K. This is made through the interception of the thermal radiation in a high thermal conductivity wrapper that surrounds the second stage and is anchored to the first stage at 80 K approximately. This radiation is dissipated in the first stage which has higher cooling power.

To reduce the absorbed and re-radiated thermal radiation in the shield, the used material should have high thermal conductivity and low emissivity at 80 K. Generally, aluminum and copper are used for the radiation shield, which have thermal

conductivities of 250 W/mK and 500 W/mK respectively. Emissivities of aluminum and copper are in the range of 0.01 to 0.078 depending on the surface finishing. Due to this variability in the emissivity it is advisable the polishing and gold/nickel-plating of the surfaces.

2.4.2. Improvement of thermal contact conductance

When two pieces are put together a thermal resistance appears in the joint. This thermal resistance depends on many factors being the effective contact surface the most important, since the real contact between pieces is made only in a series of discrete points and not in the whole surface. Even in the smoothest surfaces the contact surface is limited to some discrete points. This can be empirically checked just measuring the thermal conductivity improvement when applying more force in the joint and not when the apparent surface is increased. Therefore, to increase the force applied to a joint is the easiest way to improve the thermal conductivity.
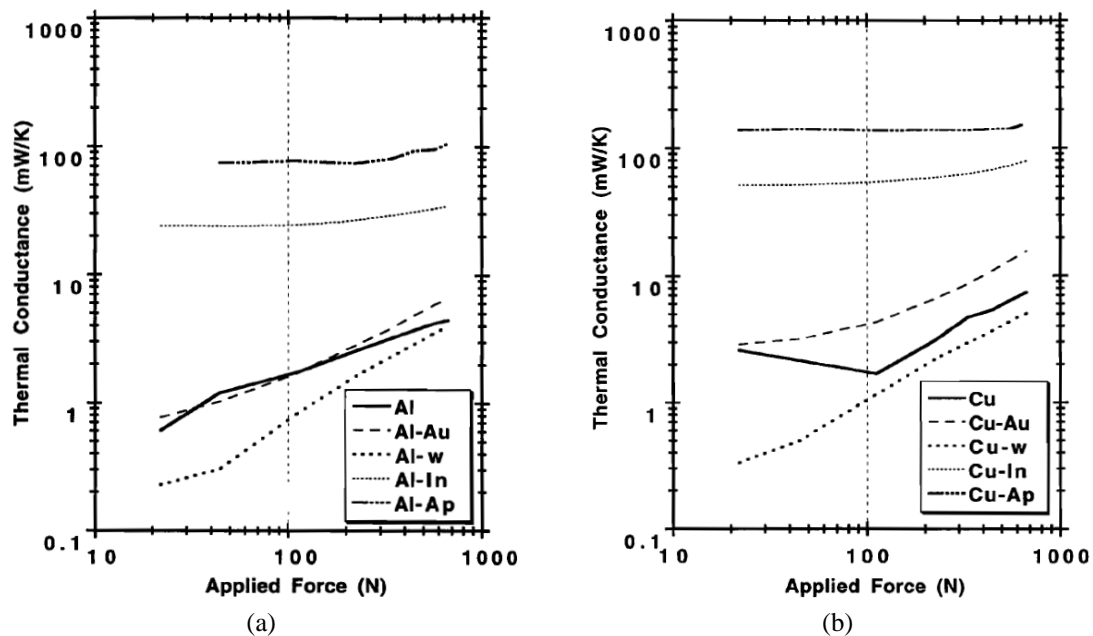
Fig. 2.9. Thermal conductance between two pieces of (a) aluminum and (b) copper as a function of the applied force and for different materials in the joint: Au – gold-plated; W – aluminum washer; In – indium foil; Ap – Apiezon® N grease [2.2].

From Fig. 2.9 it is clear that a better improvement in thermal conductivity can be achieved using appropriate materials or finishing in the joint. A soft material in the joint increases the effective contact area between pieces and then the thermal conductivity. Figure 2.10 shows the improvement in thermal conductance in the joint between two copper pieces when different materials are used at a fixed applied force.
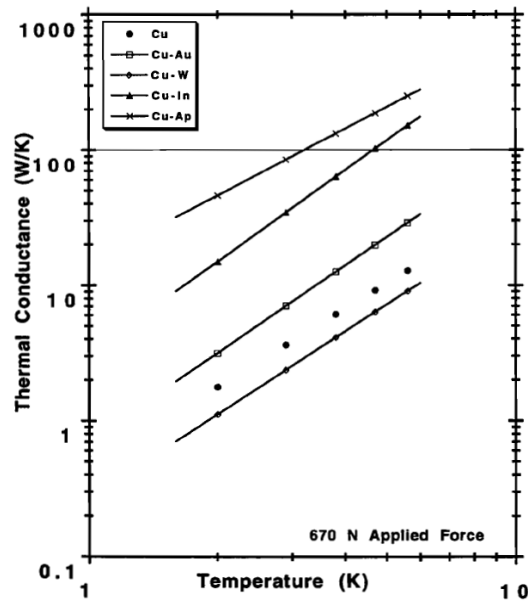
Fig. 2.10. Thermal conductance between two copper pieces with different soft materials in the joint: Au – gold-plated; W – aluminum washer; In – indium foil; Ap – Apiezon®[3] N grease [2.2].

2.4.3. Temperature sensors

There are many different types of temperature sensors: diodes (based on Si or GaAlAs technologies), temperature dependent resistors with positive or negative coefficients, thermocouples, capacitance sensors…

For applications described in this document silicon diodes are commonly used since they offer some advantages over others:

- They cover the full temperature range of interest.
- They follow a standard curve which makes them easily exchangeable.
- They have suitable accuracy without calibration.
- They are relatively affordable.
- They are available in different formats for best suit the application.

All the temperature sensors installed in the cryogenic systems presented in this document are model DT-670 from LakeShore [2.10]. They cover the temperature range 1.4 – 500 K with a typical accuracy of ±0.25 K (the uncalibrated sensors) and ±12 mK (the calibrated sensor) at cryogenic temperatures.

For the operation of these sensors a temperature controller feeds them with a DC current of 10 μA and reads the temperature dependent voltage at diode terminals. Since

---

[3] Apiezon® N is grease for cryogenic high vacuum applications. M&I Materials, Manchester, UK. www.apiezon.com

a temperature – voltage table is stored in the temperature controller the temperature value can be directly read from the controller front panel. For diode biasing and temperature read each diode is installed with four cables connected in pairs to its terminals. Due to the considerations presented in Section 2.3.1 these cables should be long, with small section, made of low thermal conductivity material and thermally anchored to the different cryostat stages.
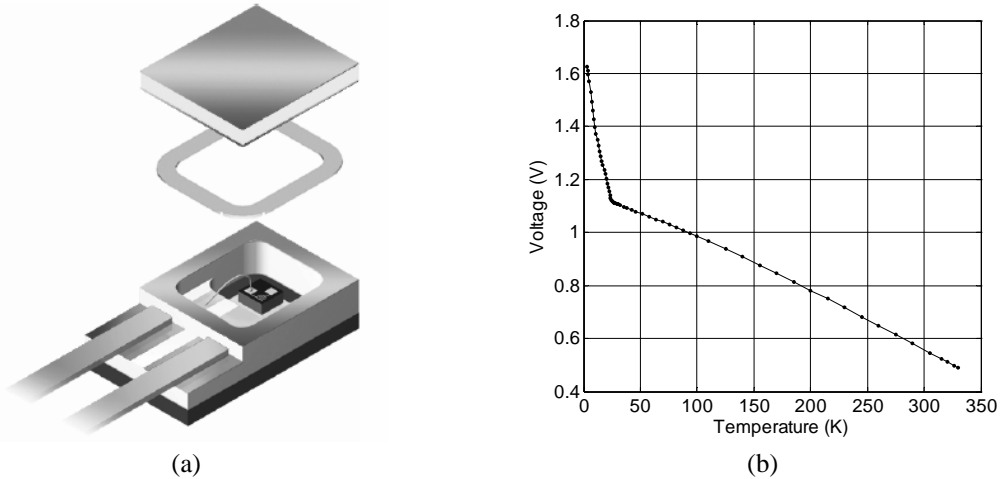

(a)   (b)

Fig. 2.11. Temperature sensor model DT-670 from LakeShore; (a) sketch of the SD format and (b) voltage – temperature standard curve.

2.5. Cryostat RF Feedthroughs

To take measurements in the cryogenic system needs the installation of proper feedthroughs in the Dewar. Measurement techniques will be explained in Chapter 3 but all of them need DC (for biasing and temperature reading) and RF (for S-parameters and noise) feedthroughs. DC feedthroughs are simple and they are not commented in this work but RF feedthroughs, both in coaxial and waveguide configurations, need some considerations regarding their vacuum and temperature isolation characteristics.

2.5.1. Coaxial RF feedthroughs

Coaxial feedthroughs enable connection between the device under test inside the cryostat and the test cables outside the cryostat using coaxial lines. Due to the small section of these coaxial lines (the higher the frequency the smaller the cable section) the conduction heat load in the cryostat second stage is small, and can be easily overtaken by the cryostat cooling power if these cables are properly anchored. Therefore, temperature isolation is not very important when considering coaxial feedthroughs.

The need to maintain vacuum inside the cryostat makes necessary the use of special adapters as feedthroughs. There are some commercial solutions for hermetic bulkhead adapters that have been reported to work properly in cryogenic environments saving the inconvenience of developing home-made feedthroughs. The cryogenic systems presented in this document are installed with model 34_SMA-50-0-3/111_NE

for measurements up to 18 GHz and model 34_SK-50-0-54/199_NE for measurements up to 40 GHz, both from Huber+Suhner. Other possibilities up to 40 GHz would be model 25-925-2040-90 from SRI and model R127.753.000 from Radiall. Coaxial hermetic adaptors for higher frequencies are not commercially available to the author's knowledge.

2.5.2. Waveguide RF feedthroughs

Waveguide feedthroughs have been designed for the WR28 band (26 – 40 GHz) based on [2.15]. The design can be divided into two different parts: a vacuum window which provides the waveguide flanges to connect the inner and outer waveguides while separates two environments with different pressures, and a thermal break made in the inner waveguide that minimizes the heat flowing to the cryostat second stage due to conduction in the waveguide body. Since the waveguide section is large the thermal load due to conduction would be too high if only heat sinks were used to reduce this load in the first and second stages. Figure 2.12 shows all the elements comprising the waveguide feedthrough.
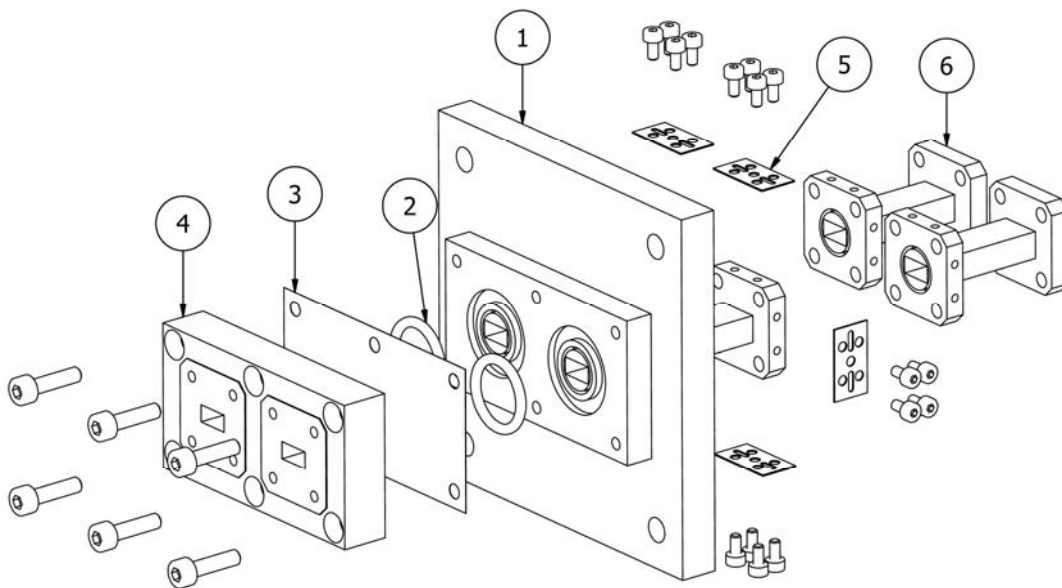
Fig. 2.12. Exploded view of the WR28 feedthrough: 1. vacuum window; 2. o-ring; 3. dielectric sheet; 4. vacuum window flange; 5. ceramic support; 6. inner waveguide with choke flange.

2.5.2.1. Vacuum window design

The main component in the vacuum window is a thin sheet of dielectric material to avoid air to go into the Dewar through the waveguide. This sheet has to be made of a material with low dielectric constant, to maintain insertion losses as low as possible, low permeability to water vapor and atmospheric gases, to maintain vacuum level along

time, and the material has to show high resistance to strain to withstand the deformation produced by the pressure differences between environments. Moreover, although in this case the waveguide section is small and therefore the infrared radiation through the window is negligible, it is advisable that this material filters as much infrared radiation as possible to avoid thermal heating of the cryostat.

In Table 2.9 some characteristics of Mylar® [2.16] are given. This dielectric is selected for the vacuum window since it has been reported to work properly for these applications despite of its high permeability to different gases compared to other materials [2.15],[2.17].

	Mylar®	Units
Dielectric constant (ε_r) @ 1GHz	2.8	
Dissipation factor ($\tan\delta$) @ 1GHz	0.008	
Ultimate tensile strength	> 20	kg/mm^2 (kpsi)
Density	1.39	gr/cm^3
Coefficient of thermal conductivity	$3.7\cdot10^{-4}$	$cm^2\cdot sec\cdot ºC$
Water vapour transmission rate @ 38ºC		
- Sheet thickness 25 µm	1.8	
- Sheet thickness 50 µm	1.1	$gr/100\ in^2/24h$
- Sheet thickness 75 µm	0.67	
- Sheet thickness 100 µm	0.42	
Permeability to Oxigen @ 25 ºC	6	$cc/100\ in^2/24h/atm/mil$
Permeability to Nitrogen @ 25 ºC	1	$cc/100\ in^2/24h/atm/mil$
Permeability to Helium @ 25 ºC	150	$cc/100\ in^2/24h/atm/mil$
Optic transmission at infrared range	~ 90 %	

Table 2.9. Electrical, physical, chemical and optical characteristics of Mylar®.

The dielectric sheet breaks the electrical continuity between the window flange and the window itself (components 1 and 4 from Fig. 2.12); therefore a gap filled with Mylar® appears in the feedthrough. This gap modifies the electrical performance of the transition producing an increase of insertion and reflection losses at some resonant frequencies within the bandwidth.

In order to overcome this problem a RF choke is designed in the vacuum window. The RF choke is a $\lambda_g/4$ deep circular slot mechanized in the waveguide flange $\lambda_g/4$ away from the waveguide cross-section. This way, a new cavity appears between flanges which can be considered as a $\lambda_g/2$ long transmission line generating a virtual shortcircuit in the discontinuity. The optimized RF choke dimensions, shown in Fig. 2.13, are $D_{in} = 8.1$ mm, $D_{out} = 9.45$ mm and $h = 2.1$ mm.
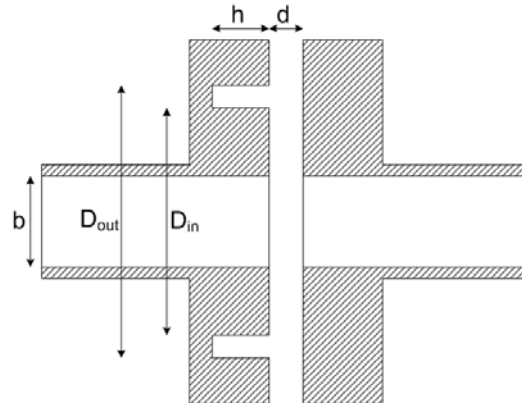
Fig. 2.13. Designed RF choke; D_{in} and D_{out} are the inner and outer diameters of the slot while h is the slot height, b is the small dimension of the waveguide (b =3.56 mm for WR28), and d is the gap produced by the dielectric sheet (dielectric thickness).

Figure 2.14 shows full 3D electromagnetic simulation results for the structure from Fig. 2.13 with different dielectric thickness, *d*, both with and without RF choke. From the results presented in Fig. 2.14 and data from Table 2.9 a dielectric thickness of 75 μm has been selected.

(a) (b)
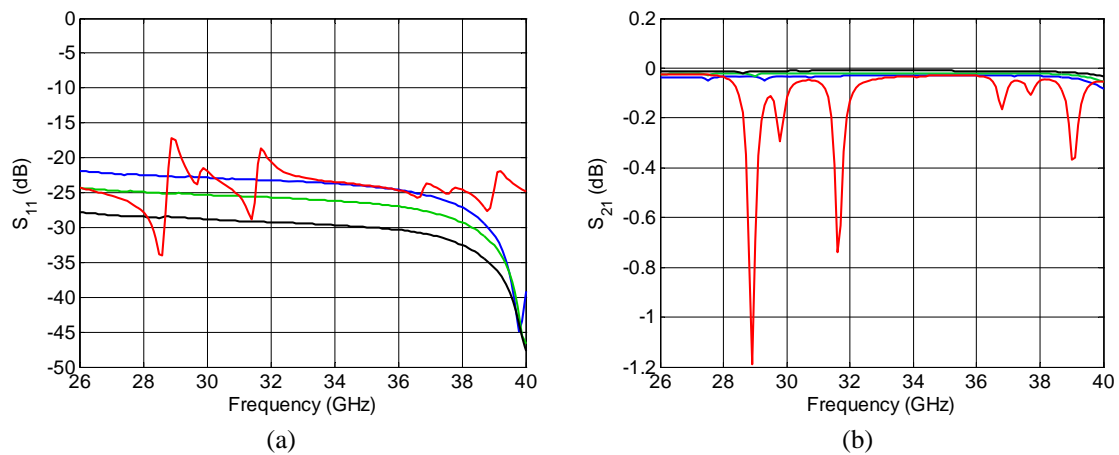
Fig. 2.14. Effect of RF choke and dielectric thickness in the window electric performance; d = 100 μm with RF choke (blue), d = 75 μm with RF choke (green), d = 75 μm without RF choke (red), d =50 μm with RF choke (black).

Finally, for the vacuum window, an o-ring is placed between the dielectric sheet and the window in order to avoid air leaks that may prevent the system to reach the low pressures needed to cool down to cryogenic temperatures. This o-ring, like the others used in the whole system, is made of fluoroelastomer (Viton®) which is suitable for cryogenic high vacuum applications since it is thermally and chemically stable.

2.5.2.2. Thermal break design

Once inside the Dewar, a new problem arises. Conduction thermal load over the second stage is too high due to the large cross-section and short length of the waveguide, which makes difficult, and sometimes prevents, to reach the minimum

desired temperature. For example, a 100 mm long WR28 waveguide connecting two stages at T_1 = 15 K and T_2 = 300 K generates a conduction thermal load of (2.4) Q = 16.2 W, if it is made of aluminum, or Q = 5.8 W, if it is made of brass. Taking into account data in Table 2.1 it is clear that the minimum temperature can not be reached with two waveguides; therefore any experiment can be performed.

The solution for reducing such a thermal load is to break the path followed by the heat by means of a vacuum gap. Theoretically, now the conduction thermal load is zero and a new radiation thermal load arises which adds to the existing radiation thermal load in the system. This new load is calculated with (2.8) and, for the temperatures considered in the previous example, we get a value of Q = 6.4 mW, if the waveguides are made of aluminum, and Q = 2.3 mW, if they are made of brass. Now, this new thermal load is negligible for the system.

To maintain the gap, i.e. to keep both waveguides separated and aligned, there is need to design suitable pieces. These pieces have to be made of a material with low thermal conductivity in order to minimize the heat flow through them. In this case ceramic supports have been designed made of the dielectric from the RO4003[4] microwave substrate. This material has a dielectric constant of ε_r = 3.55 and a thermal conductivity of K = 0.64 W/mK.

Holes are mechanized in these pieces for being screwed on to the waveguide flanges which are also mechanized with corresponding threads. Those holes define the separation between waveguides, in this case d = 100 μm. Figure 2.15 shows a sketch of the designed ceramic supports with a thickness of t = 0.4 mm.
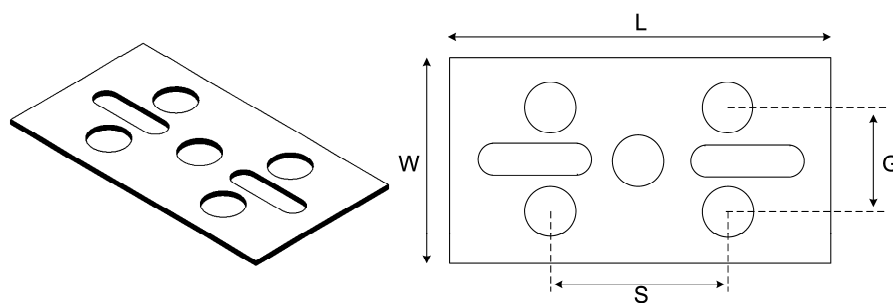

Fig. 2.15. Designed ceramic supports to keep the waveguides separated and aligned; L = 15 mm, W = 8.1 m and, S = 7 mm; G is calculated so that d = 100 μm. Additional holes are mechanized in the middle in order to reduce the piece cross-section and thus to minimize the heat flow.

The air gap between waveguide needs a RF choke mechanized in one of the flanges to avoid electrical performance degradation. Figure 2.16 presents full 3D electromagnetic simulation results of the air gap transition with and without RF choke.

---

[4] RO4003 is a high frequency laminate from Rogers Corporation. www.rogerscorp.com

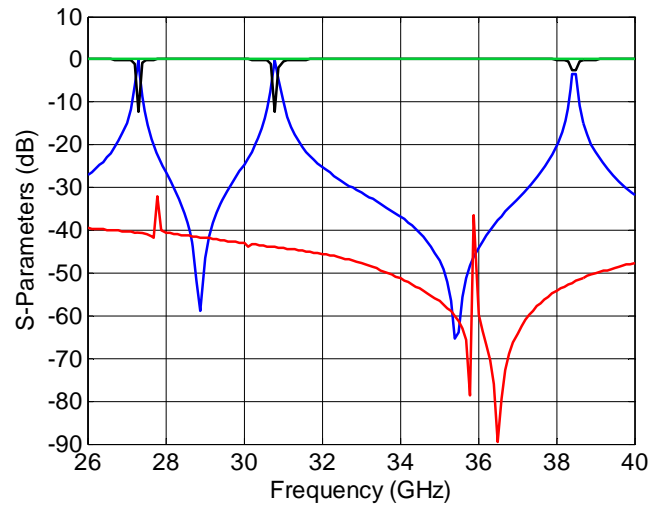The resonant frequencies within the bandwidth make necessary the inclusion of this RF choke.

Fig. 2.16. Transmission and reflection simulation results of the air gap with d = 100 μm; |S(1,1)| (blue) and |S(2,1)| (black) without RF choke, |S(1,1)| (red) and |S(2,1)| (green) with RF choke.

2.5.2.3. Measurement results

The whole waveguide feedthrough from Fig. 2.12 is characterized at room temperature with an E8364A PNA from Agilent Technologies. Measurement results are presented in Fig. 2.17, where the insertion losses of the second waveguide (element 6 of Fig. 2.12) have been leaved out since its length is variable depending on the experiment. Results show a good electrical performance with more than 21 dB return losses and around 0.1 dB insertion losses in whole WR28 band. Figure 2.18 shows the different mechanized parts that make up the feedthrough.
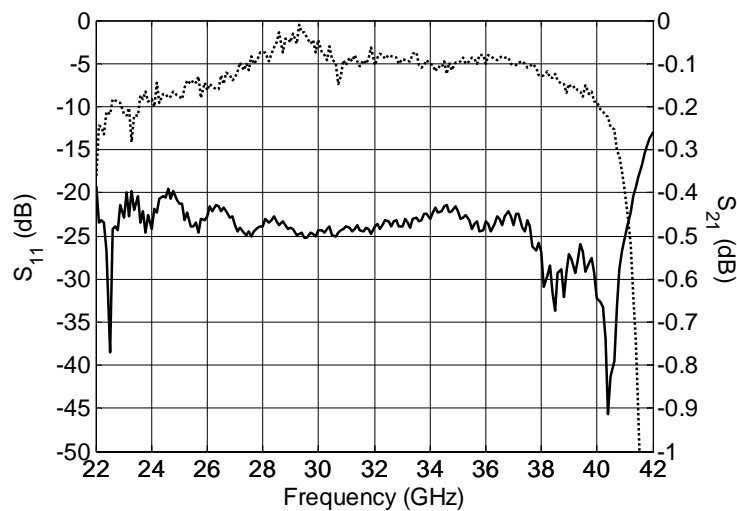

Fig. 2.17. Measurement results of the waveguide feedthrough at room temperature; |S(1,1)| solid line and |S(2,1)| dotted line.
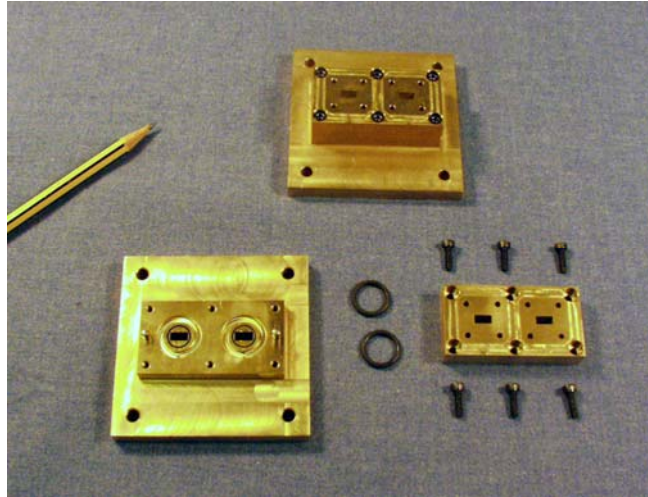
Fig. 2.18. Picture of the different components of the waveguide feedthrough.

2.6. Conclusions

This chapter has presented the problems and solutions found during this work regarding the cryogenic technology. From the design of the Dewar to the setup of the system to be used for microwave measurements, the different aspects have been covered in detail.

The different mechanisms contributing the total thermal load in the designed system have been explained and calculated. This calculation has demonstrated the inability of the first cold head, model DE-202AF, to fulfill the user requirements and therefore it has validated the acquisition of a more powerful cold head, model DE-210AE. The saving in cooling-down time achieved with the newer system is clearly stated in Fig. 2.19. Pictures of these systems both inside and outside are shown in Fig. 2.20.

On the other hand, some advices about materials and components have been given for cryogenic applications covered in this work and finally the design of a waveguide feedthrough has been presented.
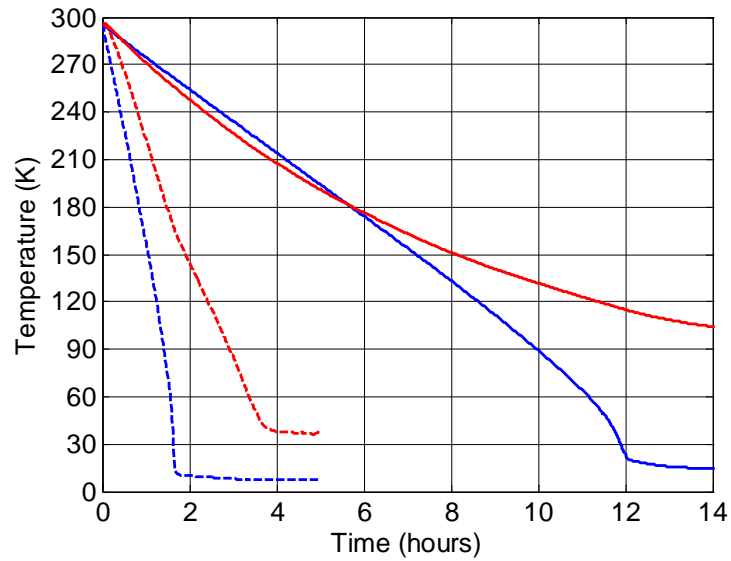
Fig. 2.19. Temperature vs. time profiles of the two cold heads in the DICOM laboratory assembled with the designed Dewar (similar for both systems) and without additional loads. The temperature in the first stage is shown in red whereas the temperature in the second stage is plotted in blue. Results for the DE-202AF system are depicted with solid lines, and results for the DE-210AE system are plotted with dashed lines. Minimum temperatures are 15 K for system DE-202AF and 7.5 K for system DE-210AE.
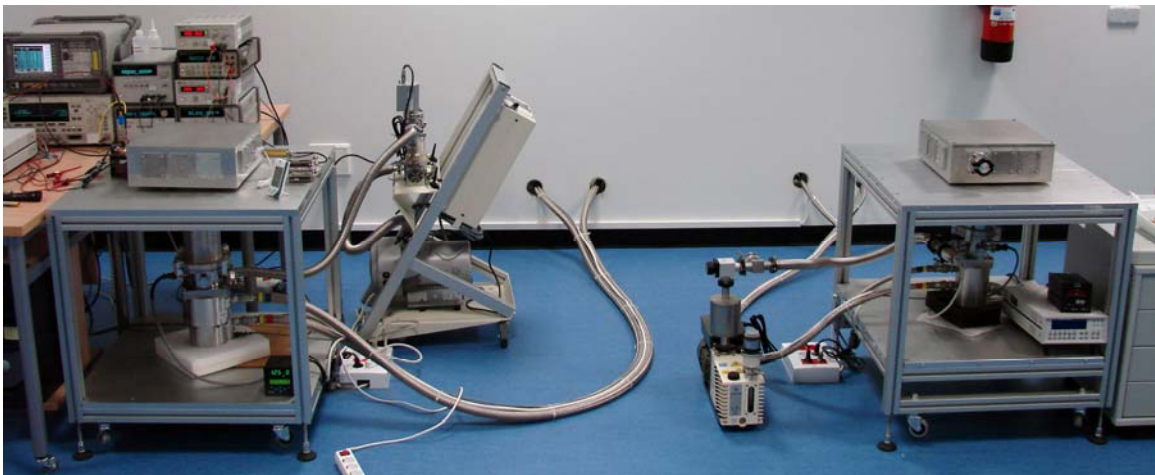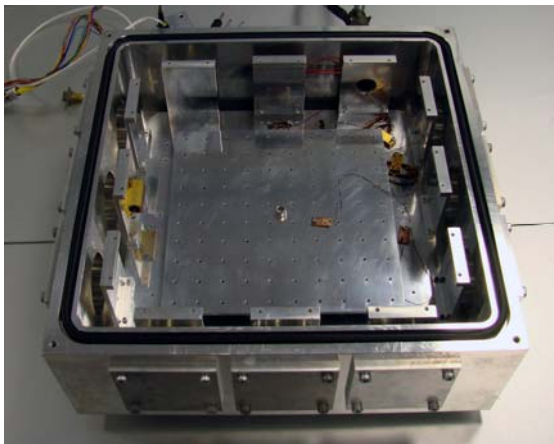
Fig. 2.20. Cryogenic systems installed in the DICOM laboratory; (a) external view of system DE-210AE (left) and system DE-202AF (right); (b) internal view of system DE-210AE; and (c) internal view of system DE-202AF.